Nano Energy 27 (2016) 595–601

Contents lists available at ScienceDirect

Nano Energy

journal homepage: www.elsevier.com/locate/nanoen

High-performance triboelectric nanogenerators with artificially well-tailored interlocked interfaces

Hak-Jong Choi [a,1], Jeong Hwan Lee [b,1], Junho Jun [a], Tae Yun Kim [b], Sang-Woo Kim [b,*], Heon Lee [a,**]

[a] Department of Materials Science and Engineering, Korea University, Seoul 02841, Republic of Korea
[b] School of Advanced Materials Science and Engineering, Sungkyunkwan University (SKKU), Suwon 440-746, Republic of Korea

ARTICLE INFO

Article history:
Received 14 June 2016
Received in revised form
3 August 2016
Accepted 6 August 2016
Available online 6 August 2016

Keywords:
Nanogenerator
Nanoimprinting
Interlocked interface
Triboelectrification
Nanostructure
High performance

ABSTRACT

We report a facile and cost-effective route for fabricating highly efficient triboelectric energy harvesters via formation of artificially well-tailored interlocked interface with a nanostructured Ni electrode and polydimethylsiloxane (PDMS). The interlocked interface formed between the nano-pillar Ni electrode and nano-pillar PDMS composite thin film effectively enhanced the triboelectricity of a triboelectric nanogenerator (TENG) by increasing the surface contact area and contact time, related to the frictional forces. The output power of four different kinds of TENGs was evaluated to confirm the effect of the surface morphology, especially the interlocked interface. A dramatic enhancement of the output voltage (~100 V) was observed with a current of up to ~23 μA. The effectiveness of the interlocked TENG (i-TENG) was also demonstrated by the greater efficiency for charging a capacitor compared with the flat-to-flat contact TENG (flat TENG).

1. Introduction

In the field of renewable energy, extensive effort has been devoted to developing effective means of harvesting natural energy such as ocean waves, wind, solar, and mechanical energy [1–4]. Specifically, mechanical energy harvesting on the basis of piezoelectricity, electrostatic interaction, and electromagnetic induction has attracted remarkable attention due to the strong potential for realizing self-powered devices and systems [5–7]. Recently, triboelectric nanogenerators (TENGs) have been investigated very intensively as a new technological concept for innovative mechanical energy harvesting based on the well-known triboelectrification phenomenon [8] that occurs between two materials with different triboelectric polarities. Furthermore, there have been many recent attempts to commercialize TENGs by increasing the output power for possible target applications, such as self-powered small electronics and sensors [7,9,10].

To achieve a high-performance TENG, the contact materials, device structures, and contact surface morphology are considered as key factors [11]. Recent strategies for achieving innovative contact materials and device structures include the development of various kinds of TENGs with a three-dimensional (3D) stacked structural design, the use of metal nanoparticles, introduction of a 2D material, etc [12–16]. Nevertheless, application of artificial control for obtaining a triboelectric active layer with a well-tailored surface morphology to achieve a dramatic increase of the output power from TENGs has been rarely attempted in spite of the importance of this approach in terms of scientific fundamentals and power-generating performance, although several approaches [17–21] such as photolithography, anodic aluminum oxide templating, and metal nanoparticle decoration have been developed to obtain controlled surface morphologies in the nanoscale and microscale ranges.

In this study, we introduce an interlocked TENG (*i*-TENG), inspired by nature's own beetle's wing [22], to increase the efficiency of TENGs for use in highly efficient energy harvesters. The i-TENG was designed and fabricated by using a nano-pillar polydimethylsiloxane (PDMS) composite thin film and a nano-pillar Ni electrode as an interlocked interface. To fabricate these structures, PDMS nano-molding and Ni electrodeposition were applied to a polyvinyl chloride (PVC) template, which offers some merits such as cost-effectiveness, large-area, and simplicity. Four different kinds of TENGs were then assembled to form different contact modes such as the flat Ni to flat PDMS contact mode (flat TENG), flat Ni to nano-pillar PDMS contact mode (np-PDMS TENG), nano-pillar Ni to flat

* Corresponding author.
** Corresponding author.
E-mail addresses: kimsw1@skku.edu (S.-W. Kim), heonlee@korea.ac.kr (H. Lee).
[1] These authors contributed equally to this work.

http://dx.doi.org/10.1016/j.nanoen.2016.08.014
2211-2855/

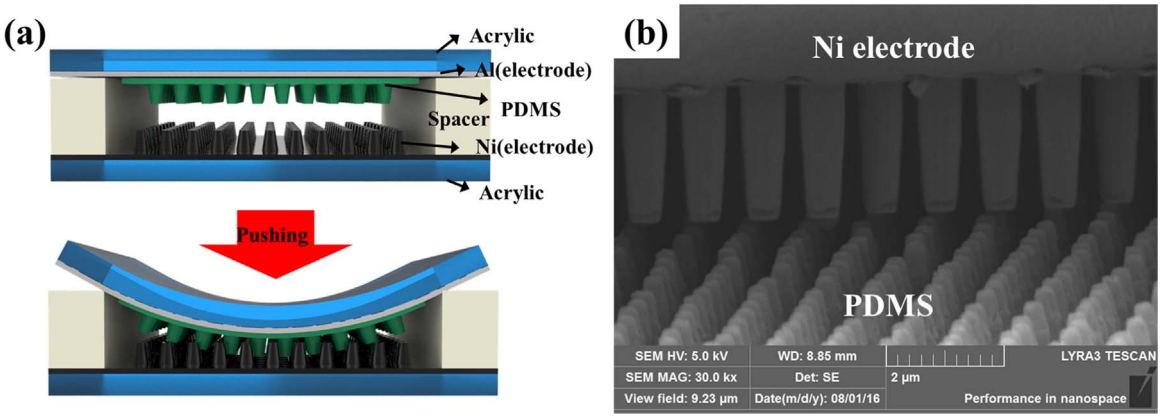

Fig. 1. (a) Schematic illustration and (b) SEM micrograph of i-TENG.

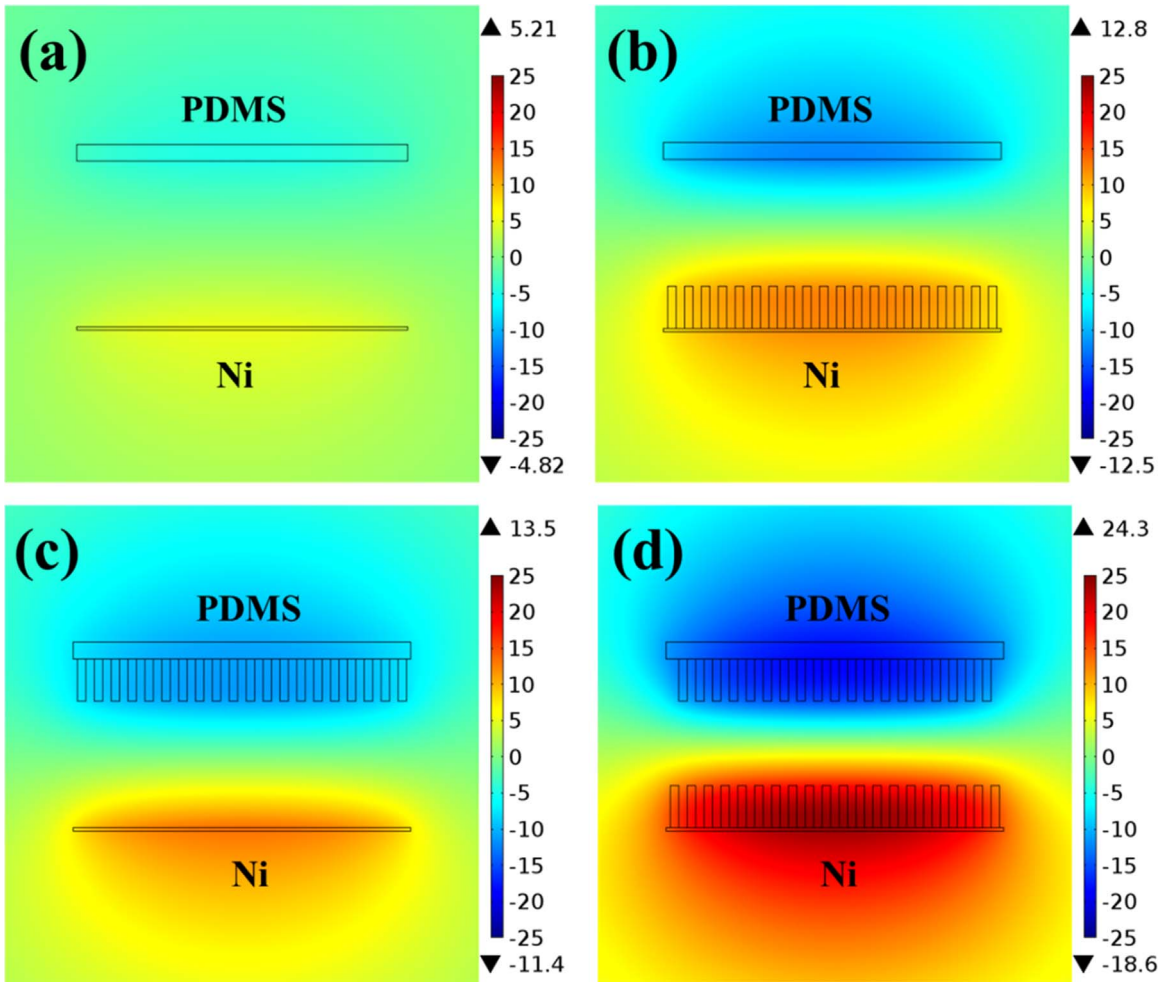

Fig. 2. Finite element simulation of vertical contact-separation modes for four different kinds of TENGs using COMSOL Multiphysics software: (a) flat TENG, (b) np-Ni TENG, (c) np-PDMS TENG, and (d) i-TENG.

PDMS contact mode (np-Ni TENG), and nano-pillar Ni to nano-pillar PDMS contact mode (i-TENG), respectively. The output voltages and currents were calculated and characterized for four different kinds of TENGs to evaluate the effect of the interlocked interface. In addition, patterned Ni electrodes with different shapes were also prepared and characterized to confirm the interlocking effect. Finally, we demonstrate the excellent power production capability of the i-TENG compared with the flat TENG by charging a commercial capacitor and illuminating light-emitting diodes (LEDs).

2. Methods

2.1. Preparation of polyvinyl chloride (PVC) template

A PVC template was used to fabricate the nano-pillar Ni and PDMS surface based on the easy detachability of the template from the Ni and PDMS surface, low-cost, and high pattern fidelity. First, a nano-pillar Si master stamp, with a pitch of 1 μm, a diameter of 0.5 μm, a height of 2 μm and square pillar array, was prepared by

using conventional photolithography and the reactive ion etching process to replicate the nano-hole PVC template (Fig. S1(a)). A fluorine-based self-assembled monolayer (SAM; heptadecafluoro-1,1,2,2-tetrahydrodecyl trichlorosilane) was coated on the surface of the Si master stamp to reduce the surface energy for easy detachment of the PVC template [23]. Subsequently, a PVC film with a thickness of 500 μm was cleaned with ethanol and deionized (DI) water and put on the nano-pillar Si master stamp. The PVC film and nano-pillar Si master stamp were placed in conformal contact using a nano-imprinting machine (Fig. S1(b)). The temperature was increased to 130 °C (above the glass transition temperature of PVC) and was maintained for 5 min. Subsequently, the PVC film and nano-pillar Si master stamp were pressurized to 10 bar for 5 min, thereby inducing deformation of the PVC film from the flat surface to the nano-hole surface (Fig. S1(c)). Finally, the machine was cooled to below the glass transition temperature of PVC (approximately room temperature (R.T.)) to stick the nano-hole pattern to the PVC surface. The nano-hole patterned PVC template was then physically detached from the nano-pillar Si master stamp. Finally, the nano-hole patterned PVC template was prepared as shown in Fig. S1(d).

2.2. Fabrication of nano-pillar PDMS composite thin film

To fabricate a nano-pillar PDMS composite thin film with high aspect ratio, 2-step nano-molding was applied to a PVC template to form the robust nano-pillar PDMS composite thin film, as shown in Fig. S2. First, hard-PDMS (h-PDMS), which has relatively high hardness, was prepared using a mixture of trimethylsiloxy-terminated vinylmethyl-siloxane-dimethylsiloxane (VDT-731, Gelest), Pt catalyst (SIP6821.1, Gelest), 2,4,6,8-tetramethyltetravinylcyclotetra-siloxane (87,927, Aldrich), and methylhydrosiloxanedimethyl-siloxane (HMS-301, Gelest) copolymers. The mixture was then spin-casted on a PVC template at 3000 rpm for 60 s. The spin-casted mixture was then cured at 65 °C for 2 h (Fig. S2(b)). Secondly, soft-PDMS (*s*-PDMS), a mixture of Sylgard 184A and 184B, was poured on the h-PDMS-coated PVC template as the backbone material. s-PDMS was then cured at 65 °C for 4 h (Fig. S2(c)). Finally, the nano-pillar PDMS composite thin film was physically detached from the PVC template (Fig. S2(d)) and observed by field-emission scanning electron microscopy (FE-SEM) to confirm successful fabrication.

2.3. Fabrication of nano-pillar Ni electrode

A nano-pillar Ni electrode was fabricated via Ni electrodeposition on a nano-hole patterned PVC template, as shown in Fig. S3. In order to apply an electrical potential to the PVC template, a Ni seed layer with a thickness of 200 nm was deposited via e-beam evaporation (Fig. S3(b)). The Ni-deposited PVC template was then transferred to a bath-type electrodeposition system with a power supply. Subsequently, the Ni-deposited PVC template and Ni plate were set as the anode and cathode, respectively. Relatively low pulsed currents (20 mA and 5 mA for forward and reverse bias) were then applied between the Ni deposited PVC template and the Ni plate to form a dense nano-pillar Ni electrode until a thickness of 100 μm was achieved (Fig. S3(c)). Finally, the nano-pillar Ni electrode was physically detached from the PVC template (Fig. S3(d)).

The nano-pillar Ni electrode was analyzed via X-ray diffraction (XRD) (Rigaku D/MAX-2500V/PC) using Cu-Kα radiation ($\lambda = 1.54$ Å); the oxidation of Ni was confirmed based on the XRD peaks of the nano-pillar Ni electrode observed at $2\theta = 44.51°$, 51.85°, and 76.37°, corresponding to the (111), (200), and (220) miller indices of Ni, as shown in Fig. 4. These results indicate that the nano-pillar Ni electrode consisted purely of face-centered cubic (FCC) structured Ni and polycrystals. The data also indicate no formation of a thick NiO film on the Ni surface.

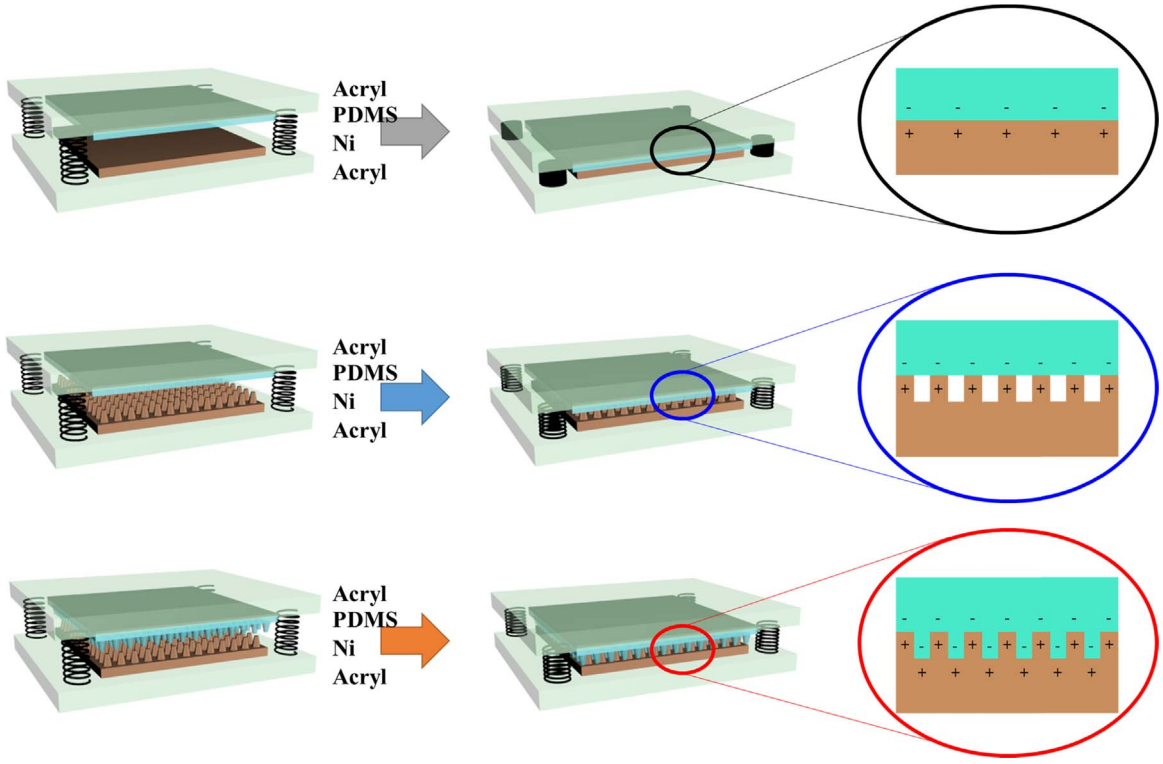

Fig. 3. Working principles for (a) flat TENG, (b) np-Ni or np-PDMS TENG, and (c) i-TENG.

3. Results and discussion

The i-TENG was operated in the typical vertical contact-separation mode and the device structure of the i-TENG was designed as shown in Fig. 1(a). For the top plate, a commercial Al tape was attached on a square acrylic polymer sheet as the top electrode. The rear side of the nano-pillar PDMS composite film was then attached to Al tape as a top contact material. For the bottom plate, the nano-pillar Ni electrode was placed on a square acrylic polymer sheet as both a bottom contact material and the bottom electrode. To maintain adequate displacement between the nano-pillar PDMS composite thin film and the nano-pillar Ni electrode, two acrylic polymer spacers were inserted between the top and bottom acrylic polymer sheet with sufficient space (approximately 0.5–1 mm). The Al tape and nano-pillar Ni electrode were connected with Cu wire to measure the output voltage and current. Fig. 1(b) shows the interlocked interface formed between the nano-pillar Ni electrode and nano-pillar PDMS composite thin film. The size of both nano-pillar structures was similar (diameter: 0.5 μm, pitch: 1 μm, height: 2 μm, and square array) due to replication of the same PVC template.

Prior to measurement and analysis of the four different kinds of TENGs, the output voltages of the TENGs were calculated by using the finite element simulation tool (COMSOL Multiphysics), as shown in Fig. 2. In this simulation work, tribo-charge density is assumed as 13.2 $\mu C/m^2$ for the four different kinds of TENG. The output voltage of the flat TENG was calculated as ~10 V, as shown in Fig. 2(a). For the np-Ni TENG, the output voltage was expected to increase to ~25 V, which is a higher value than that of the flat TENG (Fig. 2(b)). In the case of the np-PDMS TENG, a similar output voltage (approximately 25 V) was also predicted as shown in Fig. 2(c). An enormous increase in the output voltage was expected for the i-TENG, as shown in Fig. 2(d). The output voltage of the i-TENG was calculated as ~42 V, which is superior to that of the other three kinds of TENGs. This increase is attributed to the surface morphology.

To explain the effect of the surface morphology, the working principles of the TENGs are illustrated in Fig. 3. In the case of the flat TENG, the surfaces of Ni and PDMS were in normal contact in the vertical contact-separation mode, thereby generating normal friction (Fig. 3(a)). For the np-Ni or np-PDMS TENG, the nano-pillar Ni or nano-pillar PDMS structure provides a large contact area compared with that of the flat TENG. Ideally, the contact between two surfaces is larger than the contact between flat and rough surfaces in condensed matter. In the real scenario, however, perfect contact between two flat surfaces is very difficult due to various reasons, such as the difficulty in fabricating an extremely smooth surface, contact valence of the left and right side, and so on. Generally, it is well-known that a rough surface provides a larger contact area than a smooth surface [24]. Additionally, the shear friction increased because of the nano-pillar structure of Ni or PDMS, which induced high output power (Fig. 3(b)). In the case of the i-TENG, an interlocked interface was formed between the nano-pillar Ni electrode and the nano-pillar PDMS composite thin film upon contact, as shown in Fig. 3(c). Subsequently, normal and shear friction between the interface of the nano-pillar Ni and the beetle-wing-like nano-pillar PDMS led to efficient charge separation. Furthermore, the contact surface area between Ni and PDMS also increased in comparison with that of the other TENGs, which can lead to high output voltage. Thus, it is thought that the output voltage from the i-TENG is maximized due to the large surface contact area and frictional force.

Fig. 4 presents the output voltage and current of four different kinds of TENG devices in the vertical contact-separation mode, operated with an applied force of 10 kgf at a frequency of 3 Hz. The flat TENG (Fig. 4(a)) gave rise to an output voltage of approximately 8 V when the flat Ni and flat PDMS were brought into contact and separated. In the case of the np-Ni TENG and np-PDMS TENG, the output voltages increased to more than twice that of the flat TENG, with respective values of ~17 V and ~20 V. For the two different kinds of nano-pillar TENGs, a difference in the output voltage could be expected due to the difference in the surface contact area between Ni and PDMS. In the case of np-Ni TENG, the nano-pillar structure of Ni is harder than that of PDMS, which makes deformation difficult. Thus, the np-PDMS TENG should have a slightly larger surface contact area during contact and separation and a slightly higher output voltage compared to the np-Ni TENG. For the i-TENG, the output voltage was approximately 100 V, which is the highest value achieved for the four different kinds of TENGs. This high value is attributed to the interlocked interface of the nano-pillar Ni electrode and PDMS composite thin film, which generates the largest surface contact area and frictional force. When the nano-pillar Ni electrode and nano-pillar PDMS composite thin film make contact as shown in Fig. S5, normal as well as shear friction is generated, leading to a higher output voltage due to triboelectrification. Notably, based on the principle on which the i-TENG operates, shear friction is a relatively important factor for triboelectrification compared with the case of the flat TENG since there is a remarkable increase of the shear friction in the i-TENG. The output voltages for the four

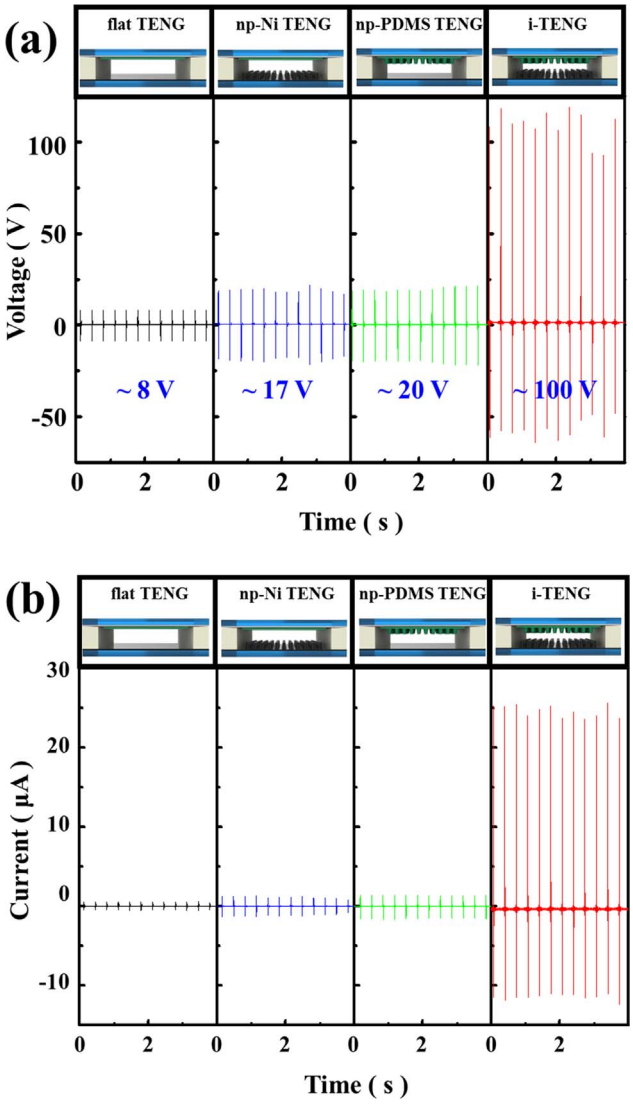

Fig. 4. Output (a) voltages and (b) currents for four different types of TENG devices.

different kinds of TENGs exhibited a similar tendency to the calculated results presented in Fig. 2, ranking in descending order as: i-TENG, np-PDMS TENG, np-Ni TENG, and flat TENG.

The output currents of the four different kinds of TENGs are shown in Fig. 4(b). The trend exhibited by the output currents was the same as that of the output voltages. For the flat TENG, an output current of 0.5 μA flowed through the external circuit when Ni and PDMS were brought into contact and separated. In the case of the np-Ni and np-PDMS TENGs, the output voltages were about 1.2 μA and 1.4 μA, respectively. Compared with these three kinds of TENGs, the i-TENG exhibited a remarkably increased output current of up to 23 μA. The output current of the i-TENG was also due to the interlocked interface. In addition, reliability of interlocked interfaces were investigated as shown in Fig. S6, which present the robust generation of output power without significant variation after 3,000 cycles of power generation. We confirmed that this interlocked interface can positively influence the output power by controlling the interface of the contact material, which makes it potentially possible to achieve high output power at the level applicable to the self-powered systems of nano-/microelectronic devices.

In order to prove the effect of the interlocked interface, three different kinds of Ni electrodes, including two kinds of nano-dot and micro-cone patterns, were fabricated using Ni electro-deposition on a PVC template. Fig. 5(a) and (b) show the nano-dot#1 and #2 electrodes with a height of 200 nm, a half pitch for diameter, and square array. The nano-dot#1 and #2 Ni electrodes had respective pitches of 400 nm and 600 nm. Fig. 5(c) shows the micro-cone Ni electrode with a bottom diameter of 2.5 μm, a height of 1.5 μm, a pitch of 3 μm, and hexagonal array. These

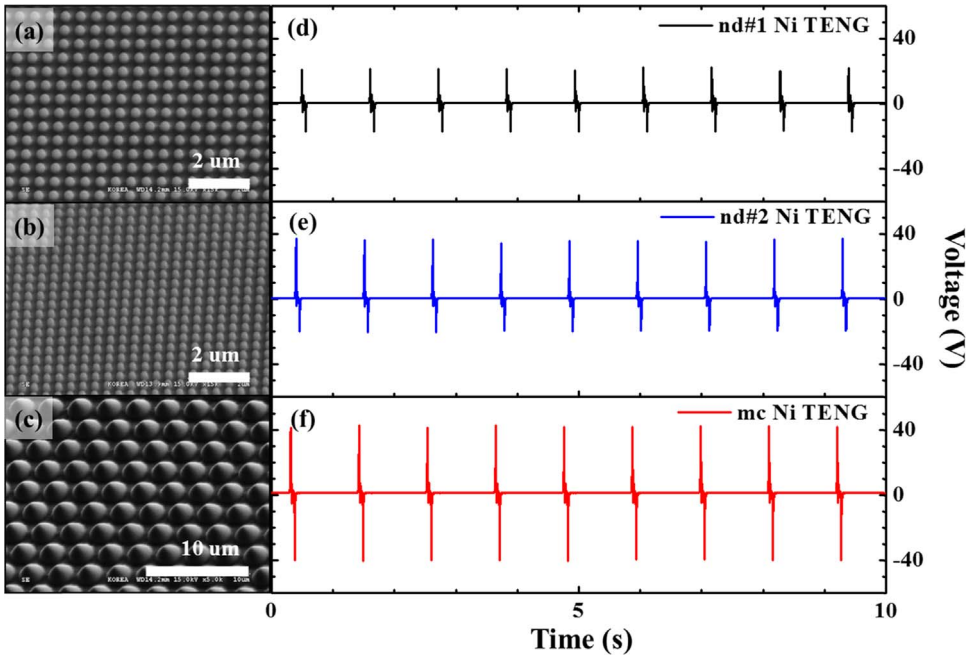

Fig. 5. SEM micrographs of (a) nano-dot#1 Ni, (b) nano-dot#2 Ni, and (c) micro-cone Ni electrodes and output voltages of (d) nd#1 Ni TENG, (e) nd#2 Ni TENG, and (c) mc Ni TENG.

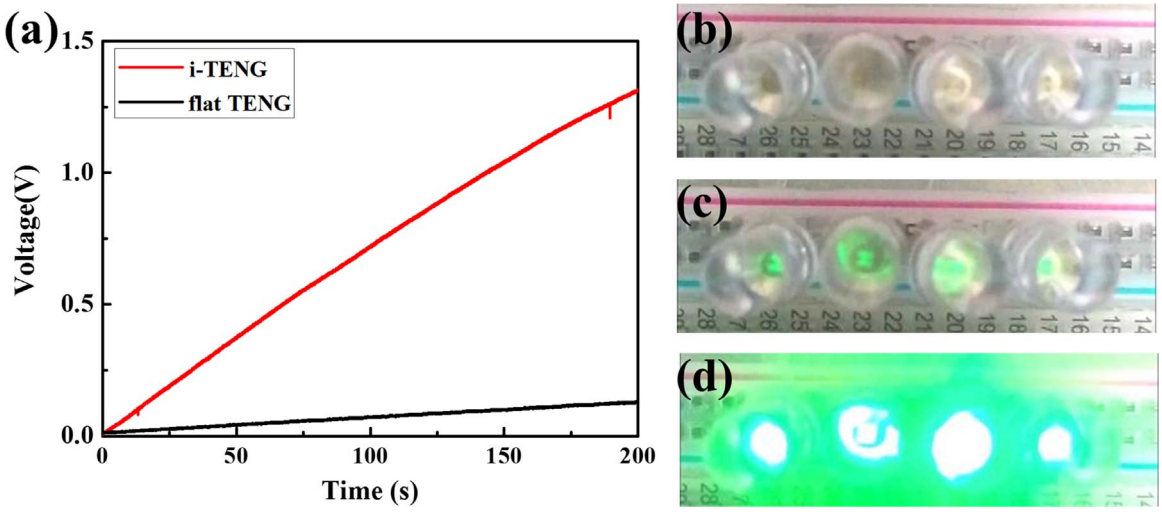

Fig. 6. (a) Charging characteristics of commercial capacitor based on output electricity generated by flat TENG and i-TENG with vibration of 10 Hz. Charging characteristics of commercial capacitor based on output electricity generated by flat TENG and i-TENG with vibration of 10 Hz. Discharging process for charged capacitor used for LED lighting: (b) setup state, operating state; (c) capacitor charged by flat TENG; and (d) i-TENG.

electrodes were assembled with the nano-pillar PDMS composite thin film as a dual-side structured TENG, including nano-dot#1 Ni TENG (nd#1 Ni TENG), nano-dot#2 Ni TENG (nd#2 Ni TENG), and micro-cone Ni TENG (mc Ni TENG). The output voltage of these three kinds of TENGs were evaluated to confirm the effect of the surface structure and to compare the difference between the interlocked interface and the other structures. The output voltage trends for nd#1, nd#2, and mc Ni TENG are summarized in Fig. 5 (d),(e) and (f). For the nd#1 Ni TENG, the output voltage was ~21 V, which is similar to that of the np-PDMS TENG. In the case of the nd#2 Ni TENG, the output voltage was ~38 V. The output voltage of the mc Ni TENG was ~42 V. These output voltages were similar or slightly higher than those of the flat, np-Ni, and np-PDMS TENGs. Compared with the i-TENG, however, the TENGs had lower output voltages. These results indirectly confirm the effectiveness of the interlocked interface.

Fig. 6(a) shows the charging characteristics of a commercial capacitor with the flat TENG and i-TENG to confirm the potential as a self-powered system for nano-/micro-devices. The commercial capacitors were charged for 200 s using the flat TENG and i-TENG. The stored energy in the capacitor was compared by analysis of the electrical potential (voltage). For the same charging time of 150 s, it was possible to charge the capacitor to over 1 V for the i-TENG, whereas for the flat TENG, the energy stored was less than 0.2 V. Thus, the i-TENG had a five-fold higher efficiency for the charging process than the flat TENG. In addition, the stored energy from the flat TENG and i-TENG were compared by illumination of LEDs. Fig. 6(b), (c) and (d) show the illumination of the LEDs from a charged capacitor by using the flat TENG and i-TENG. Four LEDs were connected in series to increase the required voltage, as shown in Fig. 6(b) (setup state). The four LEDs connected in series were directly illuminated from capacitors charged by the flat TENG and i-TENG, as shown in Fig. 6(c) and (d), respectively. By comparison of the two different operation states, we demonstrate that the capacitor charged by the i-TENG led to brighter illumination of the LEDs compared with that charged by the flat TENG. These results indicate that the interlocked interface can potentially be used as an effective method for fabricating a highly efficient TENG for self-powered systems for nano-/micro-devices.

4. Conclusions

In conclusion, we have demonstrated the high-electrical power generation performance of an i-TENG based on an interlocked interface, inspired by nature. The i-TENG was applied to a nano-pillar Ni electrode and nano-pillar PDMS composite thin film, fabricated via electrodeposition of Ni and by nano-molding of PDMS on a nano-hole PVC template. A high output voltage of 100 V and a current of 23 μA were achieved with the i-TENG, whereas the output voltage and current were only 8 V and 0.5 μA, respectively, for the flat TENG under the same mechanical compressive force of 10 kgf. Furthermore, the trend predicted by simulation was consistent with that of the measurements, even though the absolute output power values differed. Finally, the flat and i-TENG were used to charge a commercial capacitor as an example of real application. The capacitor charged by the i-TENG had a higher charging rate (over five times than that of the flat-TENG) for a given charging time. We also confirmed that the capacitor charged with the i-TENG illuminated LEDs more brightly than the capacitor charged using the flat-TENG. Therefore, we propose that the concept of the interlocked interface is potentially applicable for development of highly efficient TENGs and self-powered systems as a power sources.

Acknowledgments

H.-J. Choi and J.H. Lee contributed equally to this work. This research was supported by Nanomaterial Technology Development Program through the National Research Foundation of Korea (NRF) funded by the Ministry of Education, Science and Technology (2012M3A7B4035323) and this work was also supported by the Center for Integrated Smart Sensors funded by the Ministry of Science, ICT & Future Planning as Global Frontier Project (CISS-2011-0031870).

Appendix A. Supplementary material

Supplementary data associated with this article can be found in the online version at http://dx.doi.org/10.1016/j.nanoen.2016.08.014.

References

[1] R. Pelc, R.M. Fujita, Mar. Policy 26 (2002) 471–479.
[2] K.A. Emery, M. Green, Y. Hishikawa, W. Warta, E. Dunlop, Prog. Phtovoltaics Res. Appl 23 (2010) 1–9.
[3] N.L. Panwar, S.C. Kaushik, S. Kothari, Renew. Sustain. Energy 15 (2011) 1513–1524.
[4] L.B. Kong, T. Li, H.H. Hng, F. Boey, T. Zhang, S. Li, J. Baeyens, Energy Technol. 3 (2007) 790.
[5] X. Wang, J. Song, J. Liu, Z.L. Wang, Science 316 (2007) 102.
[6] R. Venkatasubramanian, E. Siivola, T. Colpitts, B. O'Quinn, Nature 413 (2001) 597–602.
[7] F.-R. Fan, Z.-Q. Tian, Z.L. Wang, Nano Energy (2012) 328–330.
[8] L.S. McCarty, G.M. Whitesides, Angew. Chem. 47 (2008) 2188–2207.
[9] J.H. Lee, R. Hinchet, S.K. Kim, S. Kim, S.-W. Kim, Energy Environ. Sci. 8 (2015) 3605.
[10] K.Y. Lee, J. Chun, J.-H. Lee, K.N. Kim, N.-R. Kang, J.-Y. Kim, M.H. Kim, K.-S. Shin, M.K. Gupta, J.M. Baik, S.-W. Kim, Adv. Mater. 29 (2014) 5037.
[11] Z.L. Wang, ACS Nano 7 (2013) 9533–9557.
[12] G. Zhu, J. Chen, Y. Liu, P. Bai, Y.S. Zhou, Q. Jing, C. Pan, Z.L. Wang, Nano Lett. 13 (2013) 2282–2289.
[13] W. Yang, J. Chen, X. Wen, Q. Jing, J. Yang, Y. Su, G. Zhu, W. Wu, Z.L. Wang, ACS Appl. Mater. Interfaces 6 (2014) 7479–7484.
[14] S. Kim, M.K. Gupta, K.Y. Lee, A. Sohn, T.Y. Kim, K.-S. Shin, D. Kim, S.K. Kim, K. H. Lee, H.-J. Shin, D.-W. Kim, S.-W. Kim, Adv. Mater. 26 (2014) 3918–3925.
[15] S. Wang, L. Lin, Z.L. Wang, Nano Lett. 12 (2012) 6339–6346.
[16] J. Yang, J. Chen, Y. Yang, H. Zhang, W. Yang, P. Bai, Y. Su, Z.L. Wang, Adv. Energ. Mater. 4 (2014) 1301322.
[17] G. Zhu, C. Pan, W. Guo, C.-Y. Chen, Y. Zhou, R. Yu, Z.L. Wang, Nano Lett. 12 (2012) 4960–4965.
[18] P. Bai, G. Zhu, Z.-H. Lin, Q. Jing, J. Chen, G. Zhang, J. Ma, Z.L. Wang, ACS Nano 7 (2013) 3713–3719.
[19] Z.-H. Lin, G. Zhu, Y.S. Zhou, Y. Yang, P. Bai, J. Chen, Z.L. Wang, Angew. Chem. Int. Ed. 52 (2013) 5065–5069.
[20] G. Zhu, Z.-H. Lin, Q. Jing, P. Bai, Y. Yang, Y. Zhou, Z.L. Wang, Nano Lett. 13 (2013) 847–853.
[21] F.-R. Fan, L. Lin, G. Zhu, W. Wu, R. Zhang, Z.L. Wang, Nano Lett. 12 (2012) 3109–3114.
[22] C. Pang, G. –Y. Lee, T. –I. Kim, S.M. Kim, H.N. Kim, S. –H. Ahn, K. –Y. Suh, Nat. Mater. 11 (2012) 795–807.
[23] H. –J. Choi, S. Choo, J. –H. Shin, K. –I. Kim, H. Lee, J. Phys. Chem. C 117 (2013) 24354–24359.
[24] A.K. Geim, S.V. Grigorieva, K.S. Novoselov, A.A. Zhukov, S.Y. Shapoval, Nat. Mater. 2 (2003) 461–463.

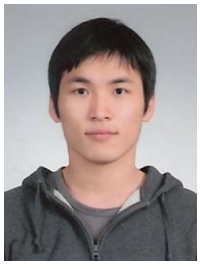

Hak-Jong Choi is a Ph.D. candidate under the supervision of Prof. Heon Lee at Department of Materials Science and Engineering in Korea University. His research interest is focused on designing and nanostructuring of functional materials for nanophotonic and energy conversion devices, such as nanogenerator, artificial photosynthesis, solar cell, and optical metamaterials.

Jeong Hwan Lee is a Ph.D. student under the supervision of Prof. Sang-Woo Kim at School of Advanced Materials Science & Engineering in Sungkyunkwan university (SKKU). His research interests include Energy Harvesters.

Junho Jun is a M.S. student under the supervision of Prof. Heon Lee at Department of Materials Science and Engineering. His research interests is focused on nanostructured electrode based on nanofabrication and nanoscale electrodeposition for the application of energy conversion devices.

Tae Yun Kim is a Ph.D. student under the supervision of Prof. Sang-Woo Kim at School of Advanced Materials Science & Engineering in Sungkyunkwan university (SKKU). His research interests include Piezoelectric FEM Simulation & Analyzation of AFM.

Prof. Sang-Woo Kim is an Associate Professor in School of Advanced Materials Science and Engineering at Sungkyunkwan University (SKKU). He received his Ph.D. from Kyoto University in Department of Electronic Science and Engineering in 2004. After working as a postdoctoral researcher at Kyoto University and University of Cambridge, he spent 4 years as an assistant professor at Kumoh National Institute of Technology. He joined the School of Advanced Materials Science and Engineering, SKKU Advanced Institute of Nanotechnology (SAINT) at SKKU in 2009. His recent research interest is focused on piezoelectric/triboelectric nanogenerators, photovoltaics, and two-dimensional nanomaterials including graphene and hexagonal boron nitride nanosheets. Now he is an Associate Editor of Nano Energy and an Executive Board Member of Advanced Electronic Materials.

Prof. Heon Lee is a Professor at Department of Materials Science and Engineering, and Director of Nano-Materials and Device Laboratory (NMDL), Pioneer Research Center for Metamaterials and Institute for Converging Technology in Korea University. He received his Ph.D. from Stanford University in Department of Materials Science and Engineering in 1996. His recent research interest is focused on the design, synthesis, and fabrication of nanomaterials and nanostructure based on unconventional nanofabrication for the applications of various nanophotonic devices and energy conversion devices, including photovoltaics, light emitting diode, artificial photosynthesis, metamaterials and energy harvester.